Challenges in mapping seismically invisible Red Fork channels,

Anadarko Basin, OK

Rachel Barber

ConocoPhillips School of Geology and Geophysics

The University of Oklahoma

ABSTRACT

The Red Fork formation is a channel system within the Anadarko Basin in west central Oklahoma. It was deposited during many different stages in the Desmoinian, and contains multiple target zones. Red Fork channels have earned their description of being "invisible" over many years of dry hole wells. Even after surprise production out of the Red Fork is encountered, attempts made to go back to seismic and track channel systems have been unsuccessful. Confusion over why the Red Fork channels are so difficult to detect is the driving force behind this study.

Attributes are a valuable tool used by interpreters to extract information contained within seismic traces. Often the information extracted by attributes is too small to be recognized by the unaided human eye. Specific attributes such as sobel filter and spectral decomposition have been used with success in the past to identify channel systems, and the recent development of enhanced curvature algorithms gave a positive outlook to Red Fork channel detection through attributes.

My attribute focused study was aided by other methods as well. The possibility of finding an empirical relationship for differentiating between sand fill and shale fill channels led to a petrophysical analysis of rock properties extracted from logs. The trends uncovered in that analysis were enhanced by comparing results from a non-producing Red Fork well to a producing Red Fork well. Amplitude variation as a result of the stratigraphic content was a question that the petrophysical comparison strove to answer.

The results of the petrophysical research suggested that a seismic inversion would be helpful in differentiating bed lithologies, specifically the 40 ft producing Red

Fork sandstone interval from Red Fork shale intervals identified in gamma ray logs from producing wells. By overlaying the gamma ray logs over the model based impedance inversion, some correlation was made linking the gamma ray identified sandstone with a small but visible low impedance feature. This interpretation led to the generation of a horizon, made with difficulty, tracking the correct interval. This horizon was then used to extract volumetric attributes.

My results aim to explain possible reasons why detection of invisible Red Fork channels has remained difficult at best, and suggest tools which might be valuable in overcoming this issue in the future.

INTRODUCTION

As one of the first producing reservoirs in the state of Oklahoma, the Red Fork was discovered near Tulsa in 1901, bringing national attention and oil fever into the Tulsa area. Red Fork channels have proved to be economic targets, and can be found in a basin with heavy well control and seismic coverage. Despite these good indications, Red Fork prospects are approached with hesitation and have become known as invisible channels due to their difficulty to be detected with existing seismic tools.

The Anadarko basin (Figure 1) has undergone extensive drilling since the discovery of the Hugoton field in the late 1960s (Fears, 1989). The plays targeted within the Anadarko Basin vary with location and may overlap. The widespread well data scattered throughout the Anadarko Basin has served as a principal guide to locate new prospects, though with erratic meandering channel deposits, the possibility of success in the Red Fork can be more trial and error than diligence and precision. For this reason 3D seismic data correlated to the well data is invaluable.

Augmenting seismic amplitude data with attributes such as spectral decomposition and coherency have been quite useful in delineating incised valley features. Peyton et al. (1998) demonstrated the strength of these two attributes in delineating both internal and external boundaries of overlapping channels. Ten years later, Suarez et al. (2008) revisited the same data volume with updated technology. Although incremental improvements such as multi-attribute blending have improved our images, gas-producing Red Fork channels remain invisible: seen in wells, but not in seismic data. The goal of this paper is to identify the reasons for the failure of the seismic method to detect these invisible channels.

I begin with a summary of the geologic depositional setting, followed by a description of the available seismic data, well logs, and production data. Next, I provide a suite of structural maps, using attributes to map faults and folds that appear to control the deposition of the Red Fork Sands. Since the Red Fork channels are seismically thin due to their fast velocity and limited seismic bandwidth, I generate and then discuss a suite of spectral components within a thin-bed tuning context. Given this framework, I then apply impedance inversion in an attempt to discriminate between the lower-impedance producing sands and the higher impedance non-producing sands. The impedance match between the producing sands and the overlying shales gives rise to these channels appearing to be 'invisible'. Although I only have access to stacked full-offset data, I use well control to conduct a simple AVO analysis that indicates that near-angle stacks may provide better discrimination than the far angle stacks. I conclude with summary maps and suggestions for improvements for future Red Fork analysis in the Anadarko Basin.

GEOLOGIC SETTING

The Red Fork formation is located in the Anadarko Basin in central NW Oklahoma and the panhandle of Texas. A Middle Pennsylvanian age deposit (Figure 2), the Red Fork is known for its varied depositional history and more recently for its invisible channels: channels that should be visible in seismic but have often proved otherwise in many surprise economic discoveries (Withrow, 1968). The Red Fork sandstone was deposited west of the Nemaha ridge in the large Enid embayment, and is part of the Cherokee Group (Withrow, 1968) (Figure 3).

The Red Fork is located above the Inola and Novi Limestone and the beneath the Pink Limestone (Figure 3). Though the complete Red Fork formation can have an overall average thickness of as much as 1500 ft, within my seismic study area the total Red Fork thickness varies between 250-400 ft, consisting of both sand and shale intervals (Janwadkar, 2004). The sand is a generally fine- to very fine-grained quartzose, but toward the base can show some coarsening upward character (Conybeare, 1976). Due to the variations of sand and shale concentration, a clean distinction of where the Red Fork ends and where the Pink Limestone begins is not always clear. Identifying sandstone channels within the Red Fork can become even more troublesome when involving thin sands amongst sandy shale.

Four stages of Red Fork deposition break down into an early period of channel sands (braided fluvial, estuarine), two phases of offshore-bar deposition during low stand sea level, and a final stage when the late seas receded from the area and channel sands were again deposited as meandering fluvial facies (Houston and Kerr, 2008, Puckette et al., 1997) (Figure 4). The variation in deposition only enhances the difficulties faced by interpreters. The Red Fork is divided into three main depositional categories: the Upper, Mid, and Lower Red Fork. The Upper Red Fork is the focus of my study in this area (the production target) which is fortunate since it is also the easiest to identify vertically in the section. Variation in composition, form, and deposition duration combined with overlapping deposition are just some of the many factors seismic interpreters must consider when working the Red Fork.

Red Fork sands in my study area consist primarily of incised valley fill deposits. Incised valleys form when the banks are cut deep enough that the flood stage of a river is not sufficient to surmount the banks. Well-defined clean channel character is seen in the gamma ray logs for the three producing wells with logs (Figure 5). Well names are differentiated with A through J given to non-producing wells, and V through Z given to producing wells. In well W, a zone of higher neutron porosity is distinguished in the lower half of the channel. Moving south, well Y shows higher porosity readings in the top and bottom of the channel, while well Z's increased sonic values indicate increased porosity in the center of the channel. Higher sonic values represent low velocity values. A low velocity interval combined with low density values (and corresponding low impedance) implies that the rock matrix is less compact which correlates to higher porosity.

DATA QUALITY

The data set used for this study consisted of a 3D seismic survey, 15 wells inside the survey, and one well with a complete suite of logs lying 15 mi outside the study area. The seismic survey is 23 mi^2 and forms part of a much larger multi-client survey shot in 2008 by CGG-Veritas. The data are of good quality, have been prestack time migrated, exhibit only slight acquisition footprint, and at the target level has a bandwidth that ranges between 10 and 80 Hz, giving a quarter wavelength resolution at the Red Fork level (V_P=16,500 ft/s) of 80 ft. Figure 6 shows a time structure map along the Red Fork production surface, and displays the available well control for this study. The Pink, Inola, and Novi limestones form coherent seismic reflection events and are easy to pick, while the Red Fork formation is more chaotic, as would be expected in a fluvial-deltaic system

(Figure 13). For this reason, I interpreted the Red Fork production surface from an acoustic impedance volume I generated, discussed in further detail later in the text.

Within the seismic study area, the wells are positioned near the center of the survey with an exception of one outlier (Figure 6). Pressure problems encountered when drilling through the Red Fork in the study area result in limited log data. To avoid the risk and cost associated with needing to fish out a logging tool, drilling companies have frequently pulled logging tools and cased through the Red Fork before logging down to deeper targets (Bob Powell, personal communication, 2-12-2010). Another obstacle encountered was that few wells contained similar log suites. Altogether, the complete log data set consists of five sonic logs, eleven gamma ray logs and four density logs, and four resistivity logs that extended at least partially through the Red Fork (Table 1). A distinction is made for 'Red Fork' production since some wells were intended for deeper formations and may in fact be economic without producing from the Red Fork. I have included both the Red Fork producing wells and the Red Fork non-producing wells on the attribute figures in an attempt to delineate patterns that may separate out one group from the other.

One well 15 mi outside the seismic study area was added for its inclusion of both a compressional and shear sonic log, and will only be mentioned in accordance with the AVO analysis.

Log data was used along with well top information to identify and separate the Pink Lime, Red Fork sandstone and Red Fork shale intervals. This was done in order to produce a velocity and density for the Pink Lime, Red Fork sandstone, and Red Fork shale intervals as well as the acoustic impedances of the layers and the boundary reflection coefficients (Table 2, 3).

The seismic data were structurally filtered to remove noise and increase higher frequency content. High frequency signal is important for differentiating thinner beds, but is often affected by poor signal-to-noise (S/N) ratios. The boosting of the S/N ratio aids in the recovery of this information. Dip-adapted (structurally oriented) filtering was selected because it does not contain windowing artifacts, and is customized for the local dip and therefore does not inadvertently remove structural signal (Helmore, 2009).

STRUCTURAL CONTROL

Novi Horizon

Figure 7a shows a time-structure map of the Novi horizon, underlying the Inola and Red Fork, which is a consistent pick across the survey. The Novi is high in the north, and becomes deeper but flattens out to the south. The most-positive and most-negative principal curvatures can be combined to generate a shape index, which indicates whether the shape is a dome, ridge, saddle, valley, or bowl, and curvedness, which indicates the degree of deformation, with zero deformation indicating a planar shape (Roberts, 2001; Mai et al., 2009). Figure 7b shows horizon slice through the coherence volume blended with shape index along the Novi, where I note trends that are consistent up through the Red Fork.

Figure 8 shows co-rendered vertical slices through amplitude and shape index volumes (both C-C’ and D-D’ locations denoted in Figure 7a. The structural complexity to the south of the study area can be seen in 8a. The shape index attribute follows the amplitude character very closely, and denotes shifts in curvature that would be difficult to identify otherwise. The channel-like feature to the north is identified in cyan (Figure 8b, black arrow), indicating a valley-shape.

Producing Red Fork Horizon

I now turn to the producing level of the Red Fork. There is no clear horizon to pick on the seismic amplitude volume. Instead, I follow Latimer et al. (2000) and generate an impedance volume (procedure shown in Appendix). Figure 9 shows a horizon slice through the model-based acoustic impedance volume along the producing Red Fork horizon. Figures 10a-d show vertical slices through the impedance volume at the producing wells and the well (well E) from which the wavelet was extracted from for the impedance generation. I also display the gamma ray log for each of these four wells so the location of the sandstone interval can be identified within the Red Fork interval. Log signatures for the three producing wells can be referenced in Figure 5, while the logs for well E are displayed in Figure 10a.

Figure 11c shows a horizon slice along the producing Red Fork through coherence blended with the structural shape and curvedness volume, where I see a meandering channel in the north. Although this channel is clearly delineated, it is not a target since the well E drilled along the west bank of the channel found only shale through the Red Fork interval. I note valley and bowl anomalies (in cyan and blue), following the path of the meander system. The impedance through the sandstone interval of well E (Figure 10a) is high, consistent with that of the AVO analysis of the producing vs non-producing Red Fork channels discussed later in the text.

After comparing the curvature results with the locations of the Red Fork producing wells, I note that these wells lie in an area of low curvedness represented by gentle dome and ridge shaped anomalies. My interpretation of this phenomenon is that the gas-charged sandstone compacted less than the surrounding shale matrix, resulting in a gentle structural high. Unfortunately, these general characteristics do not follow a clear trend, and would not be interpreted as a channel if the location was not already identified by successful Red Fork wells. Further complicating the issue is the close proximity of some dry holes to the producing wells (Figure 11, red dots).

While curvature, shape index, and coherence have little value in delineating productive sand channels, they do an excellent job of delineating shale-filled channels of little economic interest. The Red Fork producing sands remain mostly "invisible" even to more sophisticated attribute analysis.

The inline dip and crossline dip (Figures 12a and b) show directionally aligned structural features, and while identifying some channel features, they do not show a trend along the Red Fork producing wells. The most positive and most negative principal curvatures (Figures 12c and d) work together to identify channel trends. The most positive principal curvature (Figure 12c) highlights the flanks of the channels while the most negative principal curvature (Figure 12d) highlights the channel axis. The Red Fork producing wells appear to follow a channel flank trend seen in Figure 12c, suggesting a possible overbank deposit (Figure 4). Vertical slices through most positive principal curvature overlaying seismic amplitude can be seen in Figures 13a, b. A close view of where the Red Fork horizon is located displays the erratic amplitude signal. In Figure 13a, the indicated channel displays the same structural reversal seen in the shape index volume (Figure 8b) going from negative curvature beneath the Red Fork production horizon to positive curvature above.

THIN-BED TUNING AND SPECTRAL DECOMPOSITION

Widess showed in his 1973 paper "How this is a thin bed?" that the vertical resolution limit between the top and bottom of a thin bed is about 1/4 of the dominant wavelength, which at 52 Hz for the Red Fork Sandstones (V_P~16,500 ft/s) is approximately 80 ft. Spectrally whitening the data provides a high frequency of 80 Hz, suggesting that I should be able to resolve slightly thinner channels.

Kallweit and Wood (1977) showed that while it may not be possible to resolve a thin bed (distinctly see its top and bottom) it can still be detected due to lateral changes in amplitude. Spectral decomposition exploits this observation, and allows us to see tuned events as bright amplitudes and events below tuning as more subtle interference patterns, which are best interpreted on horizon, phantom horizon, or stratal slices.

Indeed, Widess (1973) points out that "A bed that is thin for one frequency is, of course, not necessarily thin for a higher frequency". For this reason I generate a suite of spectral magnitude slices sampled every 5 Hz from 10 Hz to 90 Hz and display representative images in Figure 14. In the lower frequencies, a faint indication of a NE-

SW channel can be detected coming down from the N part of the survey as well as another NE-SW oriented channel cutting across the southern end. The channel coming down from the north becomes more pronounced as the frequency content gets larger, but its presence in the lower frequencies indicates that it is a thick bed. This is verified in the seismic amplitude data (Figures 8b and 13a).

DISCUSSION

Reexamining the producing Red Fork sandstone through the acoustic impedance volume (Figure 10b-d, I note the relatively low impedance zone that corresponds to the producing wells W and Z. Not surprisingly for an incised valley, these zones are spatially limited and not always connected to each other. Block arrows indicate the higher impedance in the shale-filled channel of well E in Figure 10a. To better delineate these relatively low impedance anomalies, I compute a second derivative map of the impedance (Figure 15), which in actual implementation is the most-negative curvature of impedance along the local structural dip and azimuth. Guo et al. (2010) has shown this attribute to be very effective in correlating low impedance 'fractures' with structural lows in the Woodford Shale of the Arkoma Basin. The middle three Red Fork producing wells appear to lie along a low impedance trend.

Red Fork sandstone deposits have low amplitude and low impedance contrast with the surrounding shale. After the impedance (Z_P) cube was generated, an interpretation of the Red Fork sandstone was undertaken. Beneath the thin low-impedance Red Fork sandstone deposit (identified in gamma ray logs from Red Fork producing wells) I note a much thicker and continuous shale low impedance layer. The close proximity of these two zones makes interpretation of the thin producing sandstone difficult. The incised valley fill deposits are discontinuous, complicating a difficult surface interpretation. The thin low impedance Red Fork sandstone deposit fades in and out of view, sandwiched between a non-continuous high impedance deposit above and a strong continuous low impedance deposit below. In many instances the sandstone merges with the underlying bed or dissipates entirely before suddenly reappearing. Due to these interpretation obstacles it was very difficult to place confidence in a picked horizon. Volumetric attributes are independent of horizon picks and thereby generate more robust images than those computed from an interpreted surface. Nevertheless, I still need to identify where in the volume the "invisible" Red Fork channels lie. I believe that the surface I interpreted has good correlation with the Red Fork sandstone interval, though I also continuously verified what I was seeing in the extracted surface attributes with time slices and vertical window analyses.

ROCK PROPERTIES AND AVO – A FEASIBILITY STUDY

Because low-fold land data quality is typically inferior to higher fold marine data, AVO is less-commonly employed on land surveys than in marine surveys, particularly for Paleozoic rocks that have undergone significant lithification. Although I do not expect to see changes due to fluids (i.e. a direct hydrocarbon indicator) in such indurated rocks, I anticipate that I may be able to differentiate lithologies between high impedance tight sands, shales, and lower impedance producing sands. An amplitude versus offset (AVO) analysis is an essential part of this study in an attempt to separate out the sandstone response from the shale. The availability of a shear log in a well about 15 mi southwest of the study area permitted such rock property and AVO analysis. Though this particular well was not a Red Fork producer, it did contain the needed sandstone interval as well as overall good log range and quality.

The porosity of the channel was calculated using both the sonic and density logs. The final porosity value was generated from the density (8%).

The compressional velocity (V_P) and shear velocity (V_S) for the Pink Lime, the Red Fork sandstone, and for Red Fork shale interval just beneath the channel are shown in Table 1. The Red Fork sandstone thickness is roughly 22.5 ft and was fairly clean (Figure 3). The effective bulk modulus, K_e, and the shear modulus, G, have been determined using the following relationship:

$K_e = \rho[(V_p)^2 - {}^4/_3 V_s^2]$, and (1)

$G = \rho V_s^2$. (2)

Examining Table 2 I note that the bulk and shear moduli of the Red Fork channel are greater than those of the adjacent layers, indicating a difference between the upper and lower lithologies. The Red Fork is both stiffer (a higher effective bulk modulus) and more rigid (a higher shear modulus) than the surrounding beds.

To verify the lithology of the channel, the impedances Z_P and the Z_S have been calculated for the sandstone, the Pink Lime, and the Red Fork shale. The impedance trend of sand will normally lie above the impedance trend of shale. Figure 16 follows this behavior which indicates that the Red Fork sandstone can be differentiated using this technique.

Figure 17 shows crossplots of Z_P and Z_S versus the gamma ray log for the limestone, sandstone and shale lithologies. Based on the average gamma ray for the channel (< 80 API units), along with Z_P (> 35,000 ft/s-g/cm^3) and Z_S (> 20,000 ft/s-g/cm^3), the sandstone of the channel can be separated from the limestone and shale.

Figure 18 shows a plot of acoustic impedance versus gamma ray for a Red Fork "producing well". The similarities between the gamma ray logs in the producing wells justified combining the density log of well Y with the sonic log of well Z to synthesize the impedance of a "producing well" preserving as much original petrophysical character of the sandstone as possible. Though there is some overlap between the Red Fork sandstone, Red Fork shale, and Pink Lime, the clustering of the Red Fork shale data points above gamma ray values of 55 API and the clustering of Red Fork sandstone data points below gamma ray values of 55 API suggests that they could be separated out. However, to have gamma ray values a well already has to be in place. Acoustic impedance alone is not be a good tool for differentiating Red Fork sandstone, Red Fork shale, or Pink Lime, as the impedance values of all of these facies overlap.

Within the Red Fork, the loss of porosity and permeability is attributed to cementation by calcite and silica (Conybeare, 1976). This loss of porosity and permeability with age is often encountered in mid-North American continent rocks. The AVO response is given as

$$R_P(\theta) = b_0 + b_1 \tan^2\theta + b_2 \tan^2\theta \sin^2\theta \,, \qquad (3)$$

where

$b_0 = (^1/_2)[\Delta V_P/V_P + \Delta\rho/\rho]$,

$b_1 = (^1/_2)[(\Delta V_P/V_P) - (2V_S/V_P)^2(\Delta\rho/\rho + 2(\Delta V_S/V_S))]$,

$b_2 = (^1/_2)\ (2V_S/V_P)^2(\Delta G/G)$,

$\Delta V_P = V_{P2} - V_{P1}$,

$\Delta V_S = V_{S2} - V_{S1}$,

$\Delta\rho = \rho_2 - \rho_1$,

$\Delta G = G_2 - G_1$,

$V_P = (V_{P1} + V_{P2})/2$,

$V_S = (V_{S1} + V_{S2})/2$,

$\rho = (\rho_1 + \rho_2)/2$, and

$G = (G_1 + G_2)/2$,

with the top layer represented by subscript 1 and a bottom layer represented by subscript 2.

I tested the applicability of Rutherford and William's (1989) approximation vs. Greenberg and Castagna's (1992) equations by attempting to predict the measured shear log from the well outside to survey from its corresponding sonic and denisity logs (Table

4). I found that Greenberg and Castagna's approximation worked best, and used these values to complete the AVO analysis.

Given this data preparation, Figure 19a shows the AVO response for both the producing and non-producing Red Fork sands. The findings show the Red Fork producing well to have a shallow class three AVO character, meaning that the greatest reflectivity is at far offsets (30-45 degrees) of Red Fork sandstone whether capped by either Pink Lime and Red Fork shale.

Reexamining Figure 16, I note that the inclusion of longer offsets in non-producing Red Fork stack will lower the reflectivity, making it appear more like the producing Red Fork. I also note that the inclusion of far offsets in the producing Red Fork stack will make the stacked reflectivity less negative when overlain by the Pink Lime.

For these reasons and given the limited amplitude fidelity of land data necessary for AVO analysis, I recommend interpreting the near stack volume to better differentiate between the relatively strong positive polarity non-producing Red Fork sandstones and the relatively weak negative polarity Red Fork sandstones (Figure 19a). An AVO analysis of Pink Lime over Red Fork shale for the case of a shale filled incised valley reveals a class I response with consistent positive reflection coefficients over near, middle and far offsets (Figure 19b). This is a strong indication for why shale filled incised valley fill channels in the Red Fork are identifiable in seismic and seismic attributes while the producing incised valley was undetectable even when it's location was known.

CONCLUSIONS

Many factors contribute to the difficulty in detecting Red Fork channels in seismic amplitude and attribute data. The low impedance contrast between the sandstone channels and overlying shale and limestone is further obscured by the channel thickness of 40 ft falling beneath the tuning thickness of 80 ft. The producing channel facies were not identified with confidence in the attributes, even though other channels were clearly seen. I interpret this better imaging to a higher impedance contrast between lithologies and thicker deposition. The more clearly identified channels seen in the seismic attributes carry a strong possibility of shale infill. Well E was drilled adjacent to a N-S channel and only encountered shale.

As a result, seismic attributes might be a helpful tool in identifying high risk channel targets until technology to acquire and process higher frequency seismic data become available.

AVO studies indicate that there is a measureable impedance contrast between the overburden (Red Fork shale or Pink Lime) and underlying producing well and non-producing sandstones. However, the low impedance values of the producing Red Fork sandstone mask its identification in seismic. Gamma ray logs have been the best identification of the Red Fork sandstone, and when overlaid against the inversion, the thin low impedance sandstone body can be identified. However, the response of the thin, discontinuous low-impedance producing Red Fork sands are difficult to map. As a result, pursuing the known production using the available gamma ray logs with the inversion is still a risky proposition.

The reflectivity change in the producing Red Fork sandstone from the near offsets to the far offsets is not very large. However, the reflectivity for non-producing Red Fork sandstone has a large decrease with offset approaching the signature of the producing facies. I propose analysis of the near-offset stack to better differentiate producing from non-producing facies. Higher frequency content in the range of 120 Hz would also enhance the detection of these thin beds.

ACKNOWLEDGEMENTS

I would like to thank Bill May and Questar for inspiring this study and providing access to the well data. I thank CGG-Veritas for permission to use a portion of their multiclient survey acquired over the Anadarko Basin, and CGG-Veritas' subsidiary, Hampson-Russell, for providing the software licenses used in the model-based inversion. The interpretation and displays were generated using licenses to Sclumberger's Petrel, provided to OU for use in research and education. Financial support was provided by industrial sponsors of OU's Attribute-Assisted Seismic Processing and Interpretation consortium.

REFERENCES

Conybeare, C.E.B., 1976, Geomorphology of Oil and Gas Fields in Sandstone Bodies, 4: New York, Elsevier Scientific Pub. Co., 56-60.

Faust, L. Y., 1953, A velocity function including lithological variation. Geophysics, 18, 271-88.

Fears, R., 1989, Anadarko Basin study could revolutionize gas industry: The Journal Record, http://www.highbeam.com/doc/1P2-5479195.html; accessed 2/15/2010.

Gardner, G. H. F., W. S. French, and T. Matzuk, 1974, Elements of migration and velocity analysis**,** Geophysics, 39, 811-825

Greenberg, M.L., and Castagna, J. P., 1992, Shear-wave velocity estimation in porous rocks: Theoretical formulation, preliminary verification and applications: Gephys. Prosp. 40, 195-209.

Guo, Y., K. Zhang, K. J. Marfurt, 2010, Seismic attribute illumination of Woodford Shale faults and fractures, Arkoma Basin, OK, To be presented at the 80th International Meeting of the SEG.

Hampson, D.P., J.S. Schuelke, and J.A. Quirein, 2001, Use of multiattribute transforms to predict log properties from seismic data: Geophysics, 66, 220-236.

Helmore, S., 2009, Dealing with noise – Improving seismic whitening and seismic inversion workflows using frequency split structurally oriented filters, 79th Annual International Meeting, SEG, Expanded Abstracts, 3367-3371.

Houston, C. A., and D. R. Kerr, 2008, Sequence stratigraphy of the Red Fork Sandstone (Middle Pennsylvanian) in the vicinity of southeast Thomas, Squaw Creek, and Bridgeport Fields, Anadarko Basin, Oklahoma. http://www.searchanddiscovery.net/abstracts/html/2008/annual/abstracts/409792.htm; accessed 2/15/2010.

Janwadkar, S., 2004, Fracture pressure analysis of diagnostic pump- in tests of Red Fork sands in Western Oklahoma: Masters Thesis, University of Oklahoma, Norman.

Kallweit, R. S., and L. C. Woods, 1977, The limits of resolution of zero-phase wavelets, Presented at the 47th Annual International SEG meeting, Calgary, Geophysics, **47**, 1035-1046.

Latimer, R. B., R. Davidson, and P. van Riel, 2000, An interpreter's guide to understanding and working with seismic derived acoustic impedance data: The Leading Edge, **19**, 242–256.

Mai, H. T., K. J. Marfurt, S. Chavez-Perez, 2009, Coherence and volumetric curvatures and their spatial relationship to faults and folds, an example from Chicontepec basin, Mexico, 79th Annual International Meeting, SEG, Expanded Abstracts, 1063-1067.

Marfurt, K.J., H. Mai, 2009, Running AASPI Software with GUIs, The University of Oklahoma, AASPI, 141.

Molina, B., Red River on the Texas Oklahoma boarder, © Terra Photographs. Accessed 5/13/2010. www.geologyclass.org/Stream%20Concepts_files/image006.jpg

Northcutt, R. A., and J. A. Campbell, 1988, Geologic provinces of Oklahoma, Oklahoma Geologic Survey. http://www.okgeosurvey1.gov/level2/geology/ok.geo.provinces.small.gif; accessed 2/15/2010

New Mexico and Arizona Land Company, LLC, 2005, Anadarko Basin regional cross section, © NZ Legacy.

Peyton, L., R. Bottjer, and G. Partyka, 1998, Interpretation of incised valleys using new 3D seismic techniques: A case history using spectral decomposition and coherency, The Leading Edge, **17,** 1294-1298.

Puckette, J. O., C. Anderson, and Z. Al-Shaieb, 1997,_The deep-marine Red Fork Sandstone; a submarine-fan complex, (in Marine clastics in the southern Midcontinent, symposium, *Johnson, ed*, OGS Circular, **103**, p. 105-118**.**

Roberts, A., 2001, Curvature attributes and their application to 3D interpretated horizons: First Break, **19**, 85-100.

Rutherford, S.R., and Williams, R.H., 1989, Amplitude-versus-offset variations in gas sands: Geophysics, v. 54, p. 680-688.

Suarez, Y., K.J. Marfurt, and M. Falk, 2008, Seismic attribute-assisted interpretation of channel geometries and infill lithology: A case study of Anadarko Basin Red Fork channels, 78th Annual International Meeting, SEG, Expanded Abstracts, 1-4. Widess, M.B., 1973, How thin is a thin bed? GEOPHYSICS, **38**, 1176-1180.

Withrow, P. C., 1968, Depositional environments of Pennsylvanian Red Fork Sandstone in northeastern Anadarko Basin, Oklahoma, AAPG Bulletin, **52**, 1638-1654.

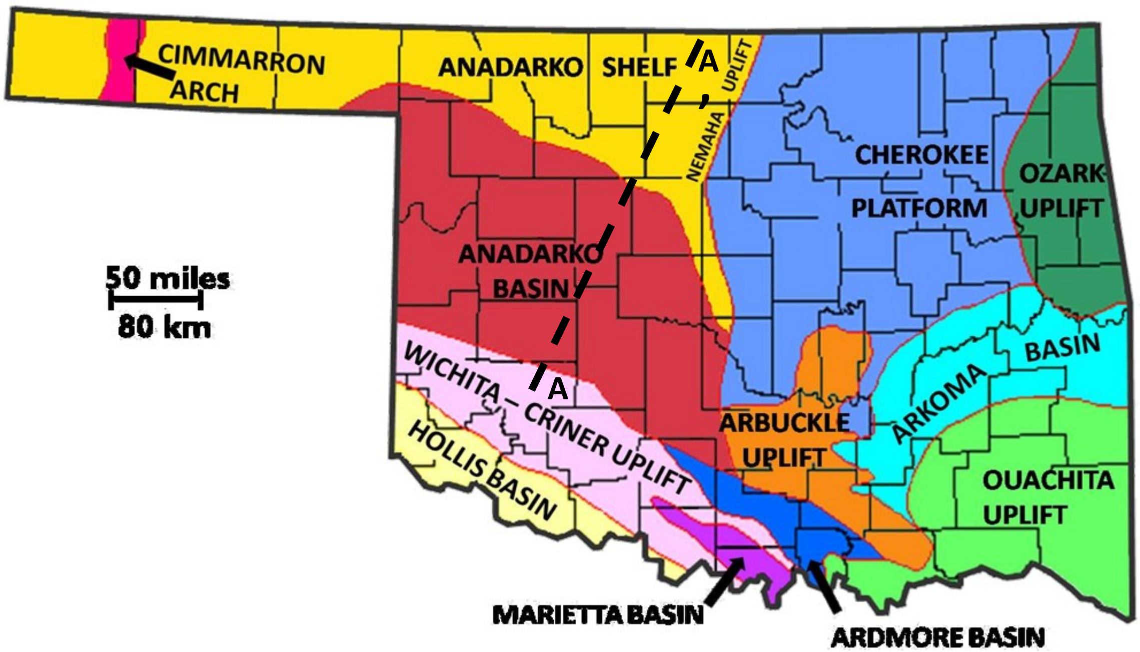

Figure 1. The study area is in the middle of the Anadarko Basin, western Oklahoma (modified from Northcutt and Campbell, 1988). Geologic section A-A' is shown in Figure 2.

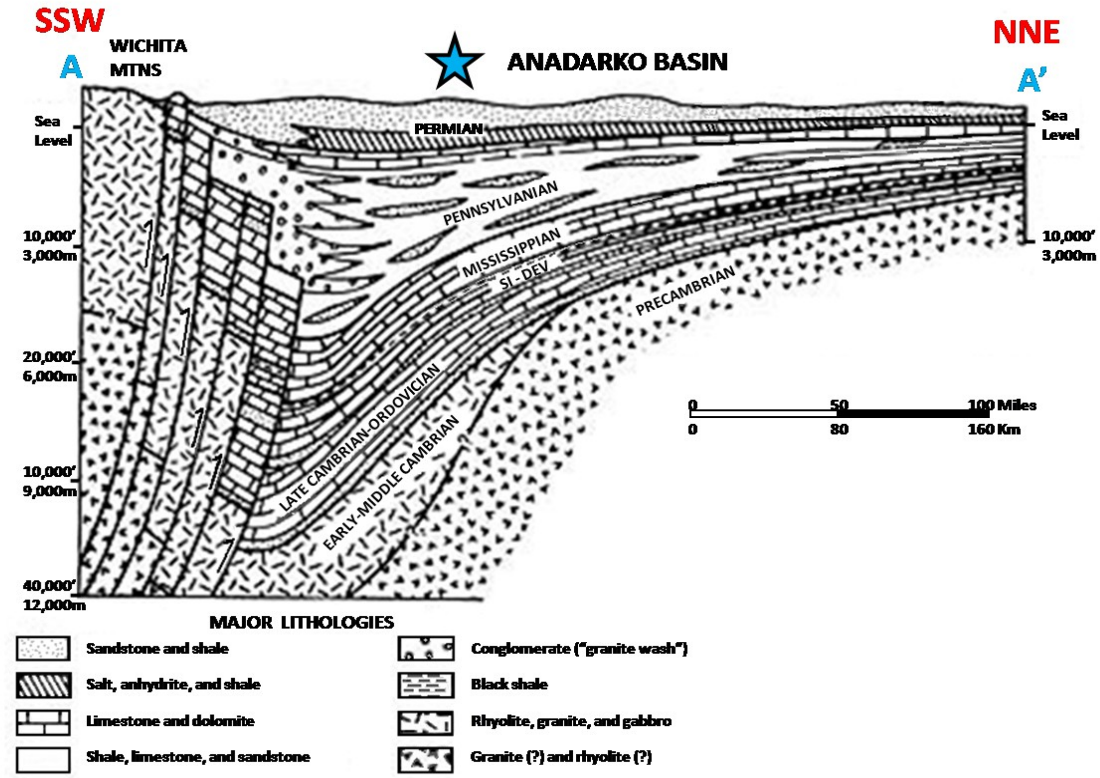

Figure 2. A SSW-NNE regional cross section through the Anadarko Basin indicated AA' on Figure 1. The Red Fork is Mid Pennsylvanian in age, and is composed of shale, limestone and sandstone. The blue star approximates the location of the study area within the basin. (New Mexico and Arizona Land Company, 2005)

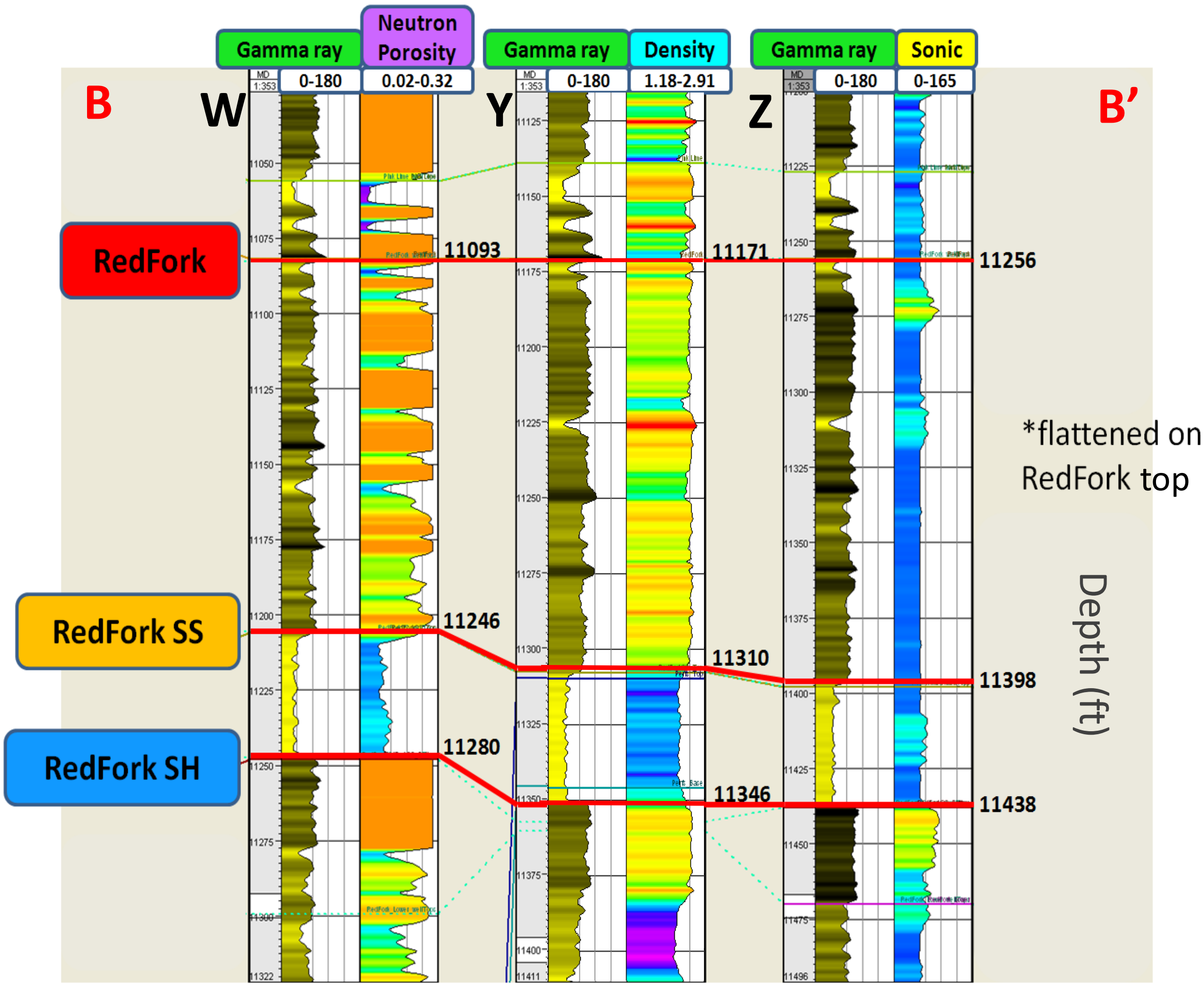

Figure 3. Cross section showing the producing Red Fork sandstone as seen in the three producing wells which contained logs: W, Y, and Z. Despite the modest log control, the correlation in the gamma ray logs are clear. Location of wells shown in Figure 4. The neutron porosity for well W indicates higher porosity to the south of the sandstone interval. The density log for well Y shows decreased density in the top and bottom of the channel, indicating similar porosity zoning to well W. Well Z shows high sonic values in the middle of the channel, indicating low velocity and suggesting higher porosity. The change in sandstone porosity from wells W and Y to Z is a reminder of the difficulty in detecting meandering RF channels due to their erratic depositional circumstances.

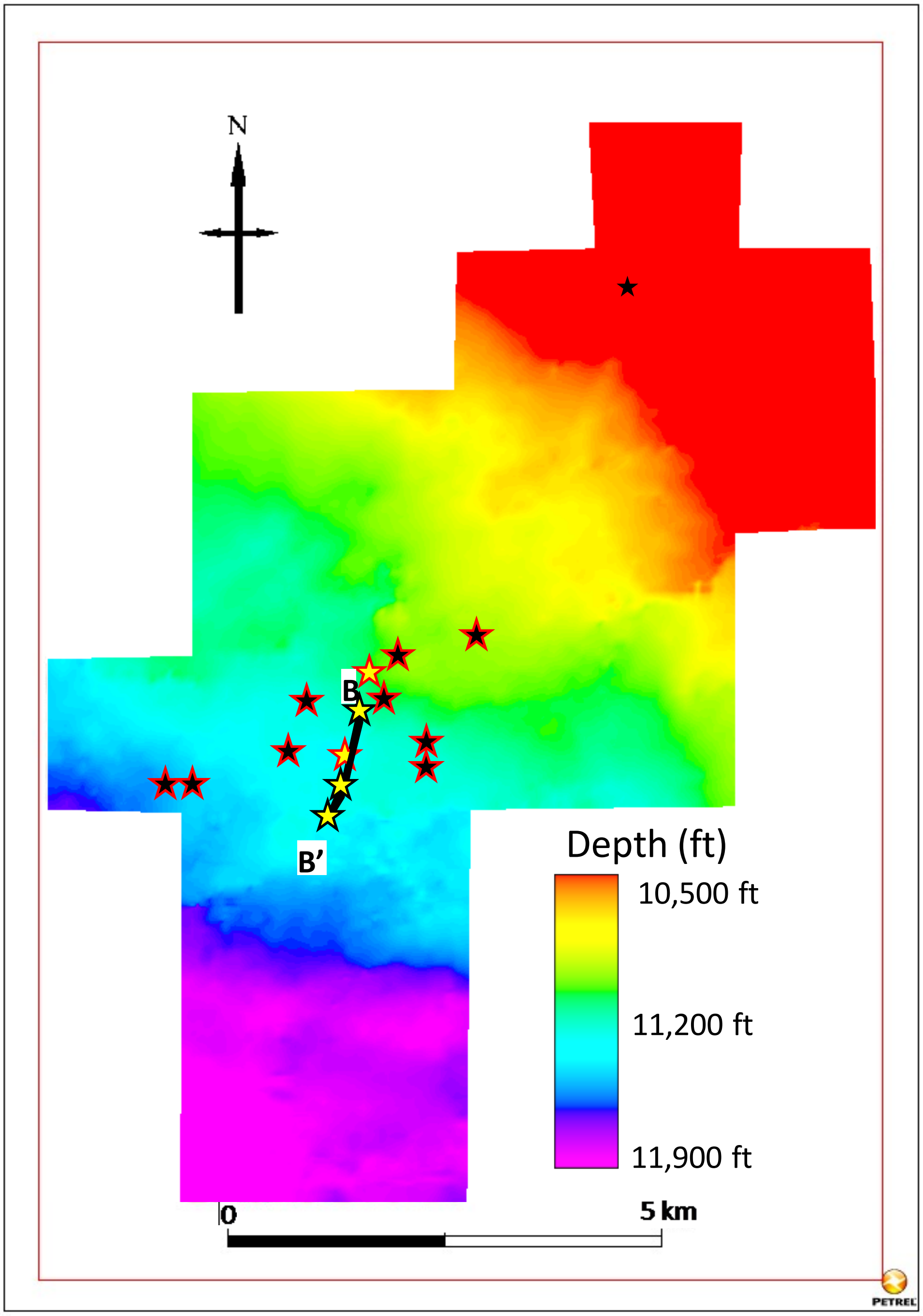

Figure 4. Time structure map of the interpreted Red Fork production surface, interpreted from the acoustic impedance (Z_P) volume. Producing wells are displayed as yellow stars and non-producing wells as black stars. The wells included in the cross section B to B' shown in Figure 3 are represented as yellow stars outlined in black. Seismic data courtesy of CCG-Veritas.

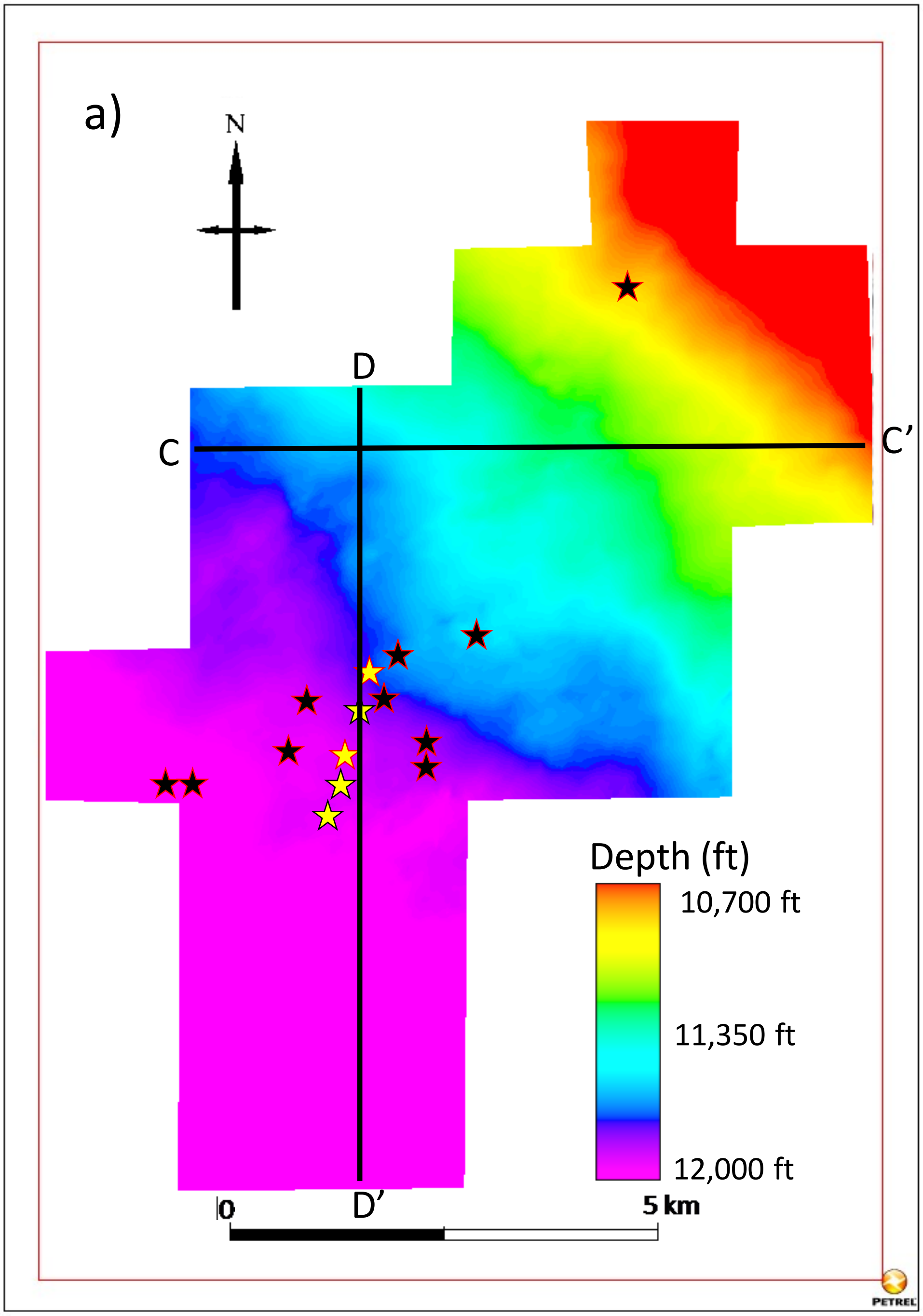

Figure 5. a) Time structure map the along Novi horizon. Producing wells are displayed as yellow stars and the non-producing wells are displayed as black stars. The wells included in the cross section B to B' shown in Figure 3 are represented as yellow stars outlined in black. Lines CC' and DD' displayed in Figure 6. Seismic data courtesy of CCG-Veritas.

b)

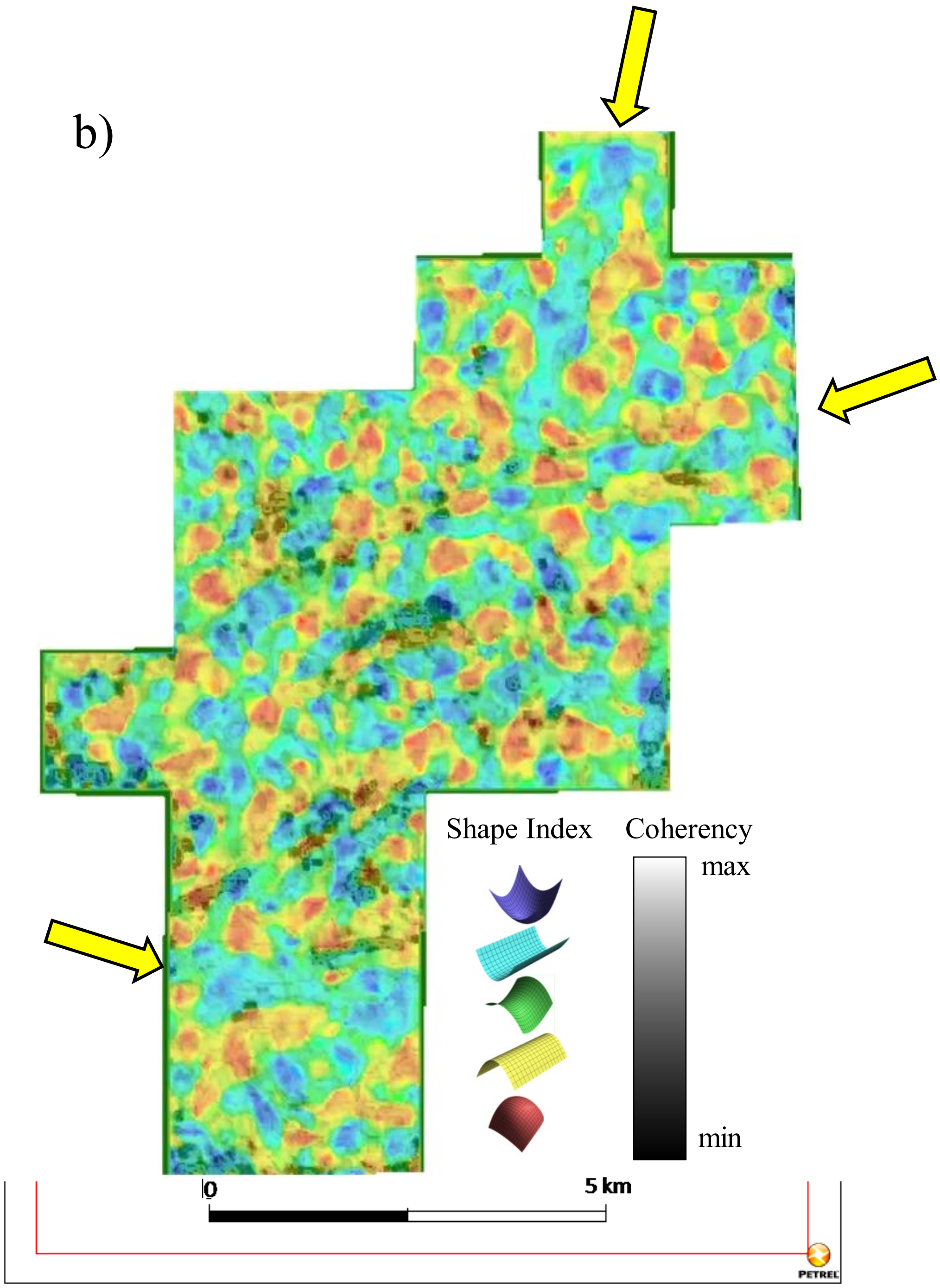

Figure 5. b) Horizon slice along the Novi through the coherence blended with shape volumes. Many trends seen in the Novi are mirrored in the Red Fork. A few of these are referenced by yellow arrows. Seismic data courtesy of CCG-Veritas.

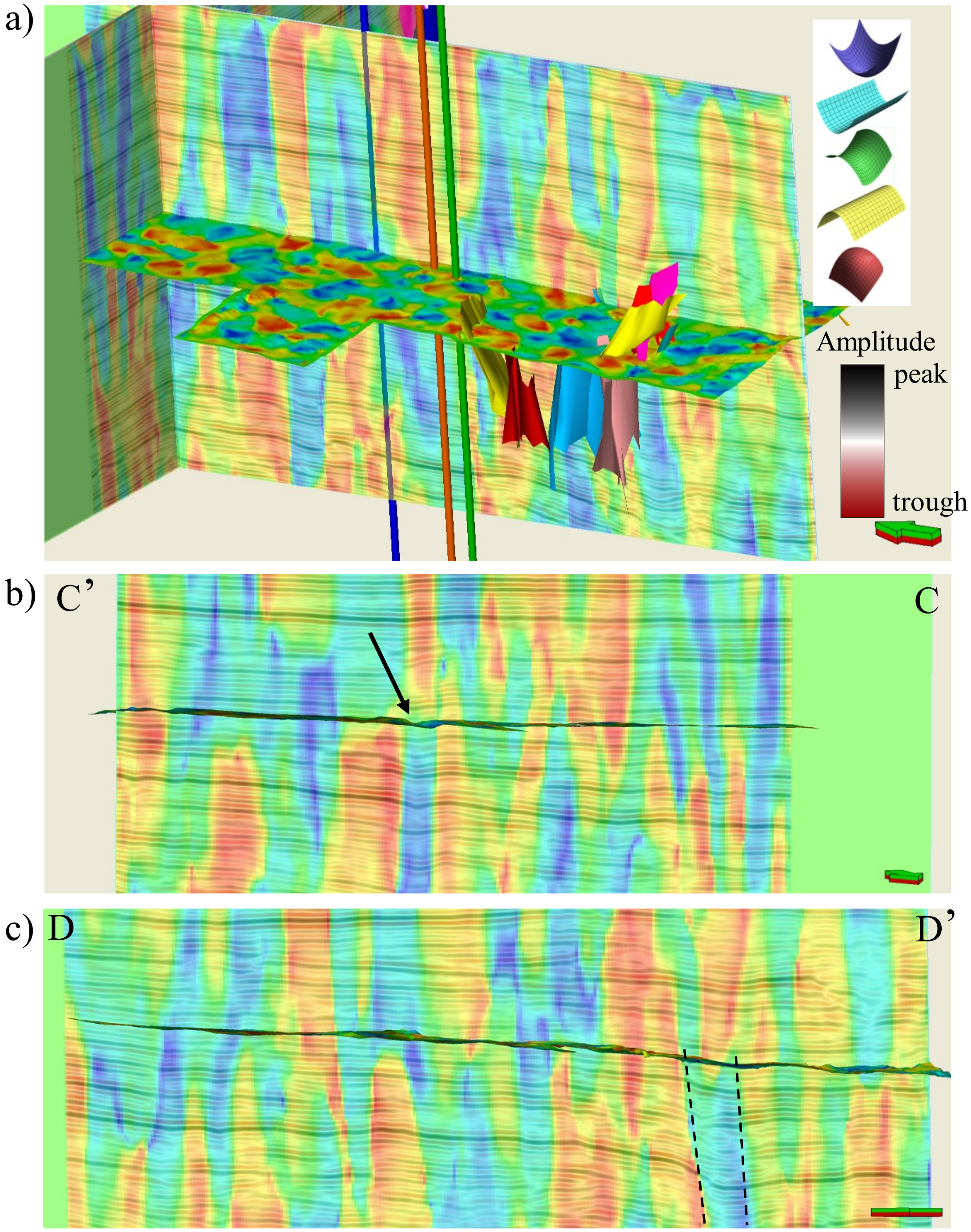

Figure 6. a) Vertical slices through structural shape co-rendered with seismic amplitude showing major faults in the data volume: b) line CC' and c) line DD'. Faults indicated by dashed black lines. The surface displayed is Red Fork production. The well bore location of well W (blue), Y (orange), and Z (green) are displayed in a). A channel can be easily seen in vertical section C-C' (black arrow), verified by the shape index cyan coloring, indicating valley shape. It is interesting to note that below the RF producing horizon, the structural character of the channel bed is bowl shaped while above the horizon the character quickly changes into a dome anomaly. Seismic data courtesy of CCG-Veritas.

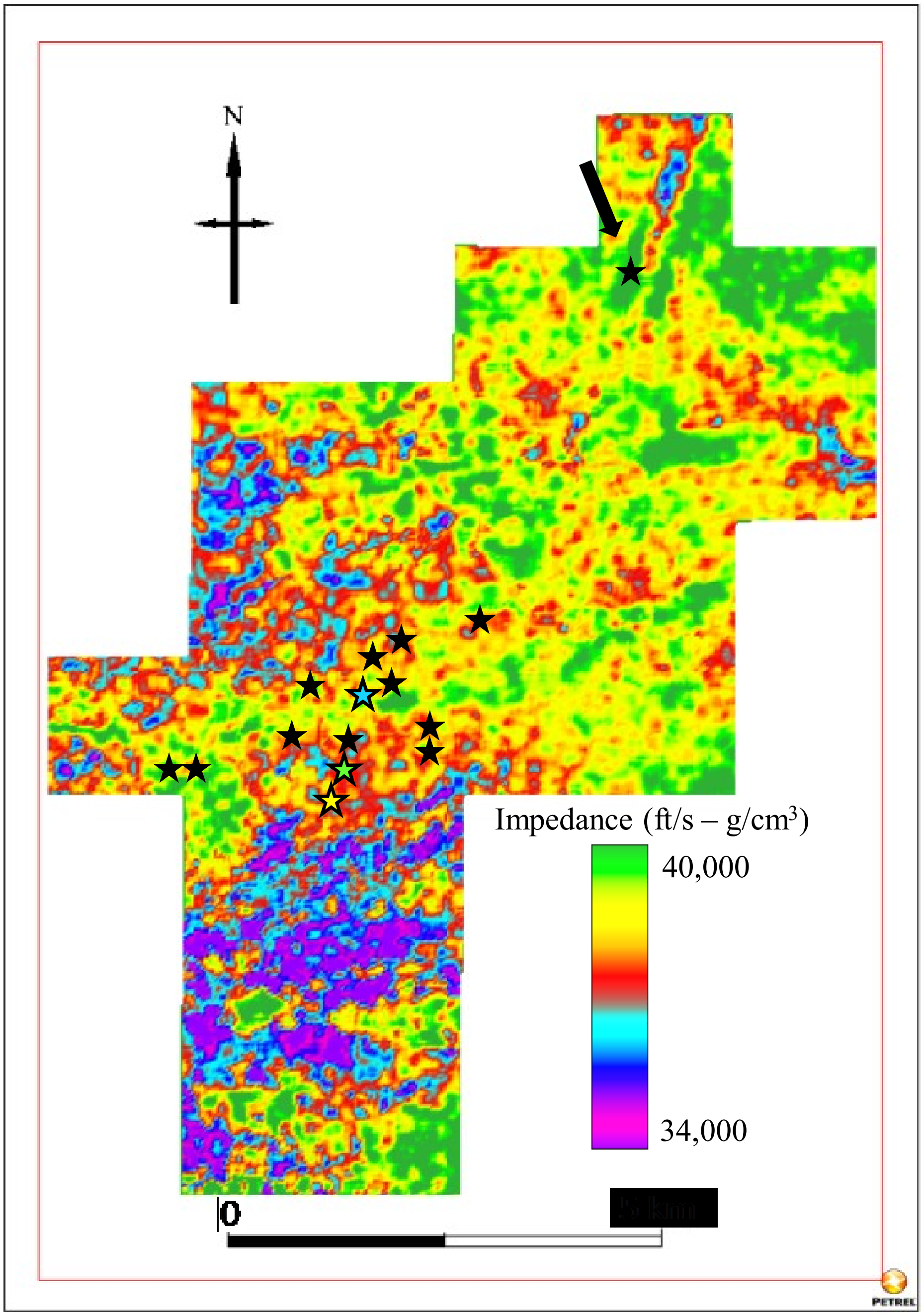

Figure 7. Red Fork horizon through impedance showing the location of wells W (blue star), Y (green star), and Z (yellow star). See Figure 3 for a log correlation of these three wells. The black arrow indicates the zone of high impedance that the non-producing well lies in. Seismic data courtesy of CCG-Veritas.

a) Well W

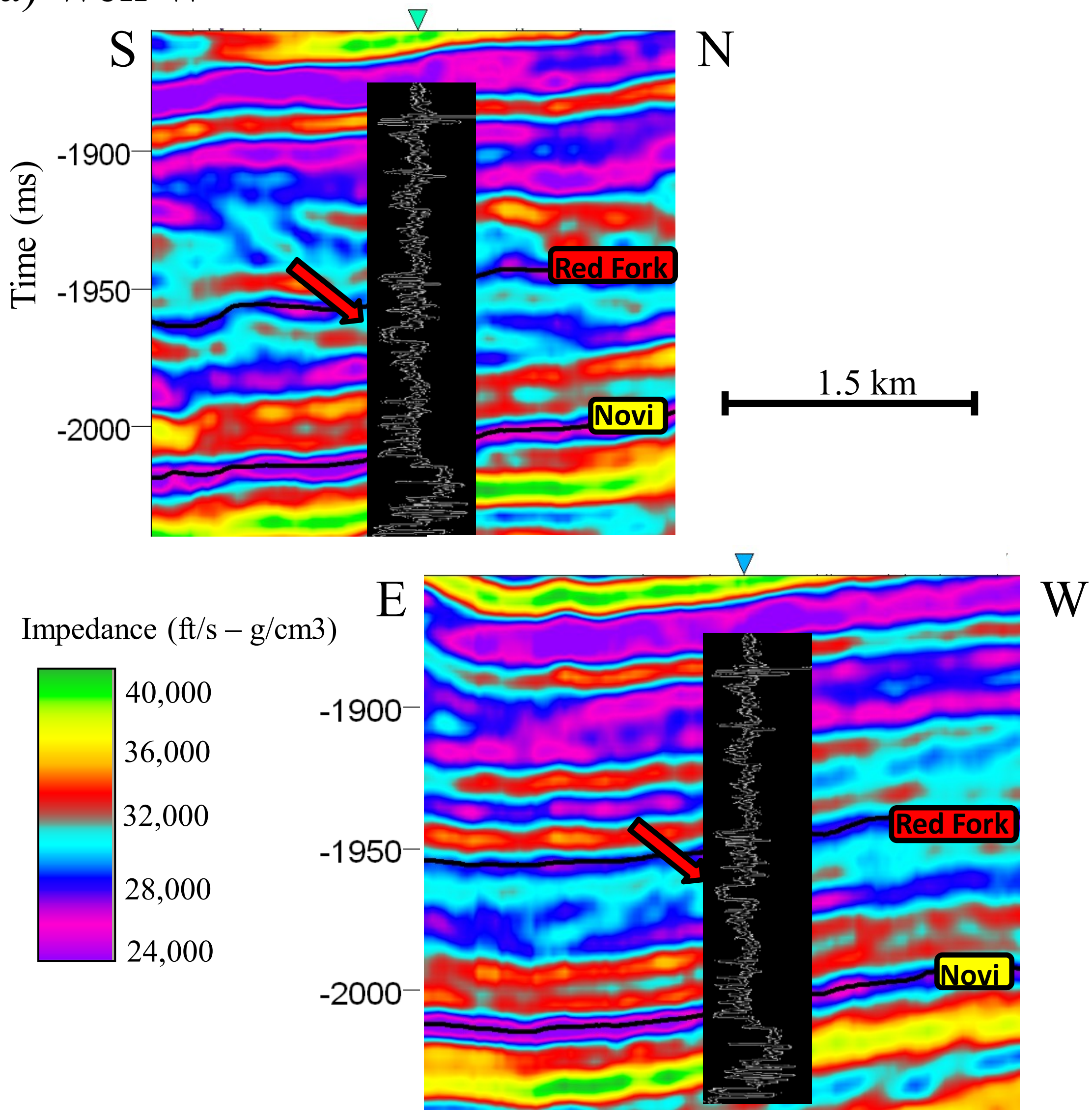

Figure 8. a) N-S and E-W vertical slices through the acoustic impedance volume, intersecting at a) well W, b) well Y, and c) well Z. The sandstone level is indicated by low gamma ray (block arrow) and low acoustic impedance (cyan to dark blue). Seismic data courtesy of CCG-Veritas.

b) Well Y

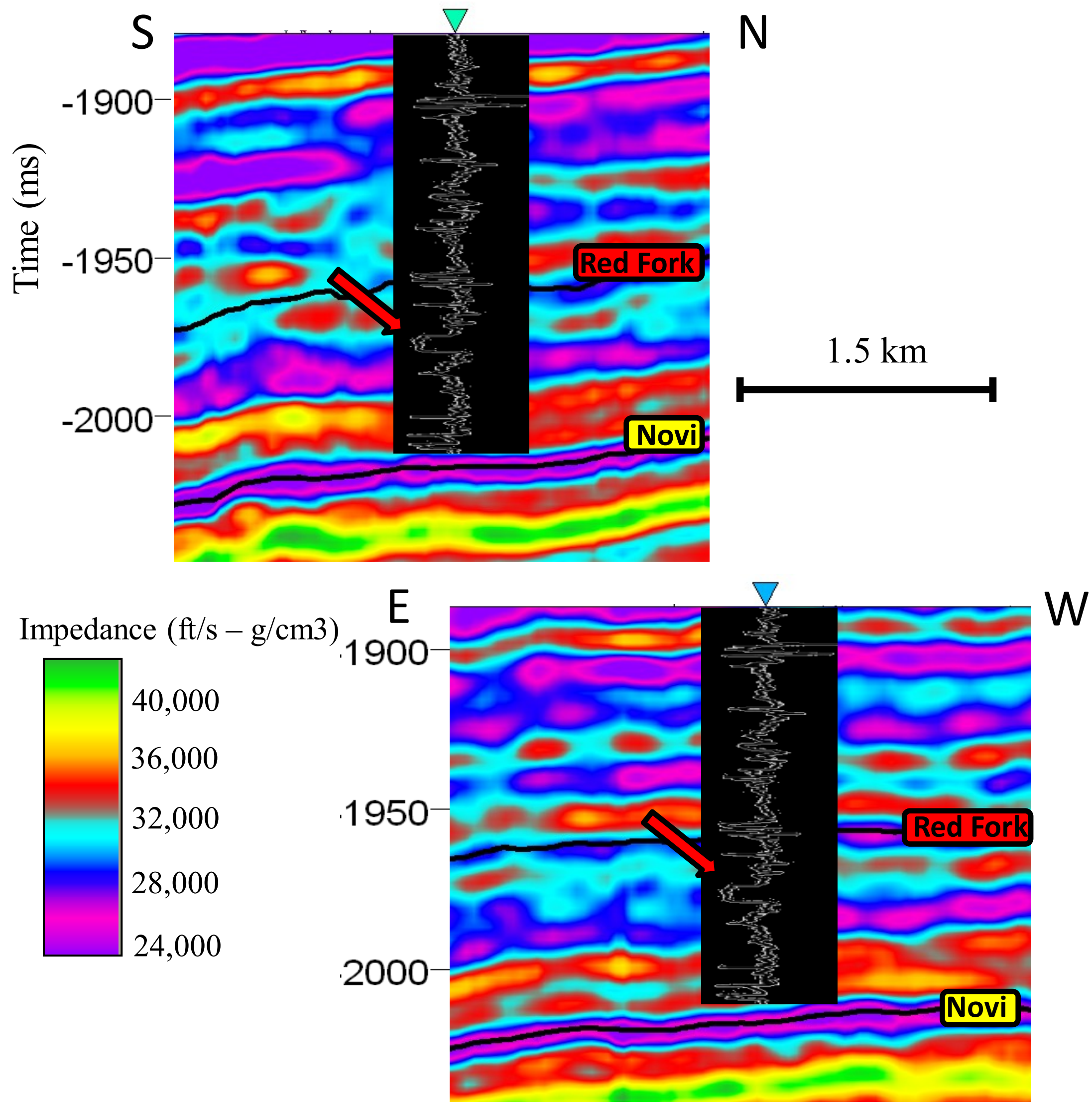

S
N
-1900
-1950
-2000
Time (ms)
Red Fork
Novi
1.5 km
E
W
1900
1950
2000
Impedance (ft/s – g/cm3)
40,000
36,000
32,000
28,000
24,000

c) Well Z

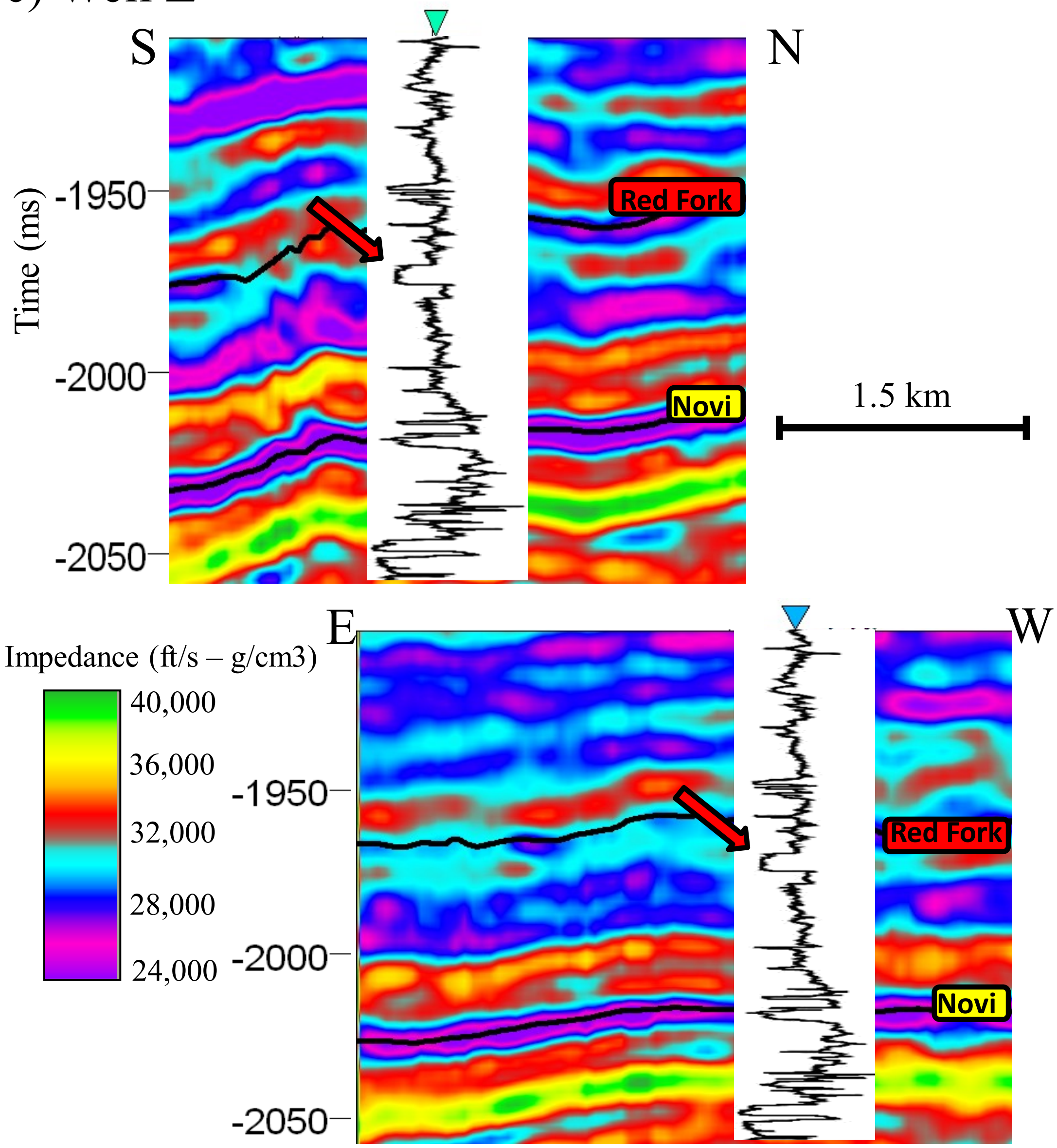

S
N
Time (ms)
-1950
-2000
-2050
Red Fork
Novi
1.5 km
E
W
Impedance (ft/s – g/cm3)
40,000
36,000
32,000
28,000
24,000
-1950
-2000
-2050
Red Fork
Novi

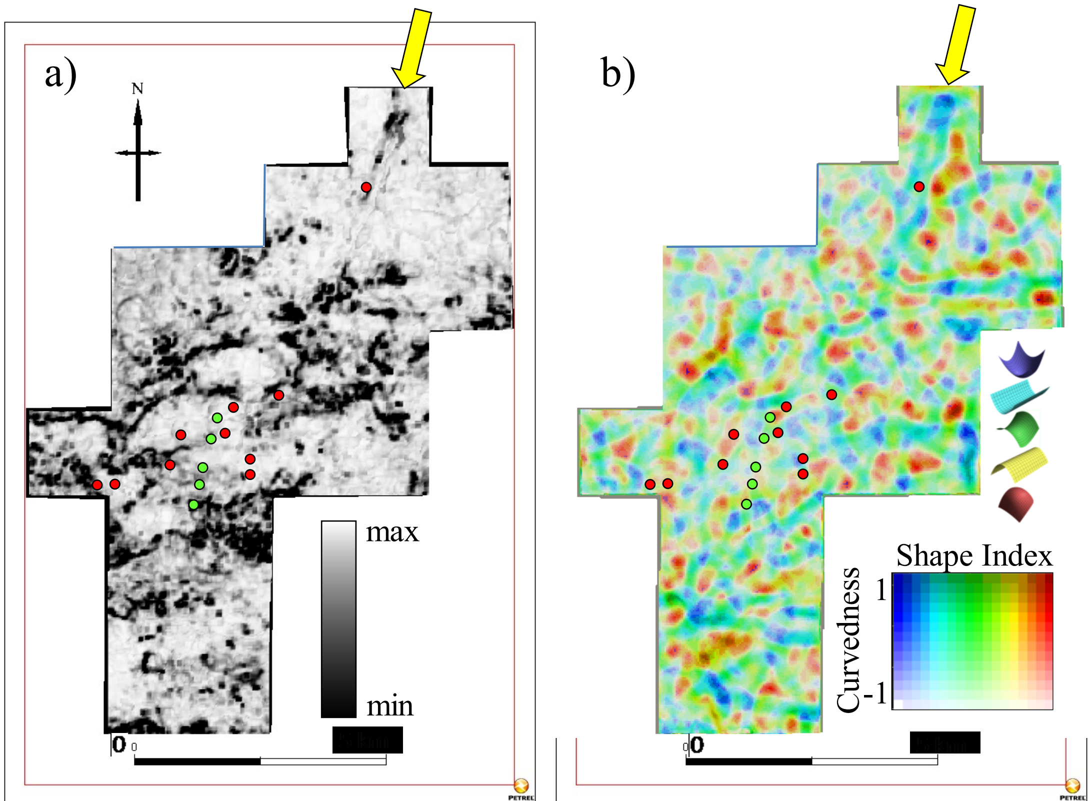

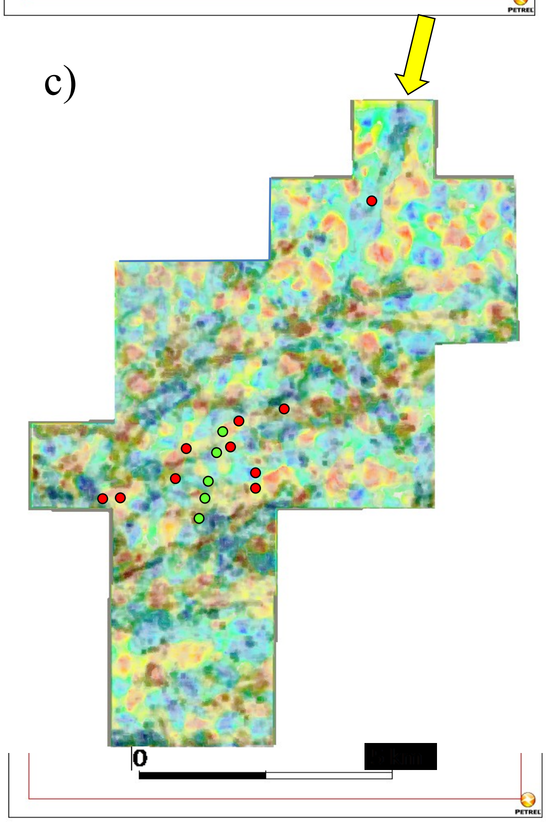

Figure 9. Red Fork production surface displaying: a) coherency, b) shape vs. curvedness and c) blended coherency with shape vs. curvedness. The edge effects picked up by the coherency line up with shape trends identified in the shape index vs. curvedness. RF producing wells are indicated by green dots and non-RF producing wells are indicated by red dots. The RF producing wells lie in an area of low curvedness with dome and ridge shape characteristics. The yellow arrow denotes the ability of both coherency and shape to identify the channel extending down from the north. Seismic data courtesy of CCG-Veritas.

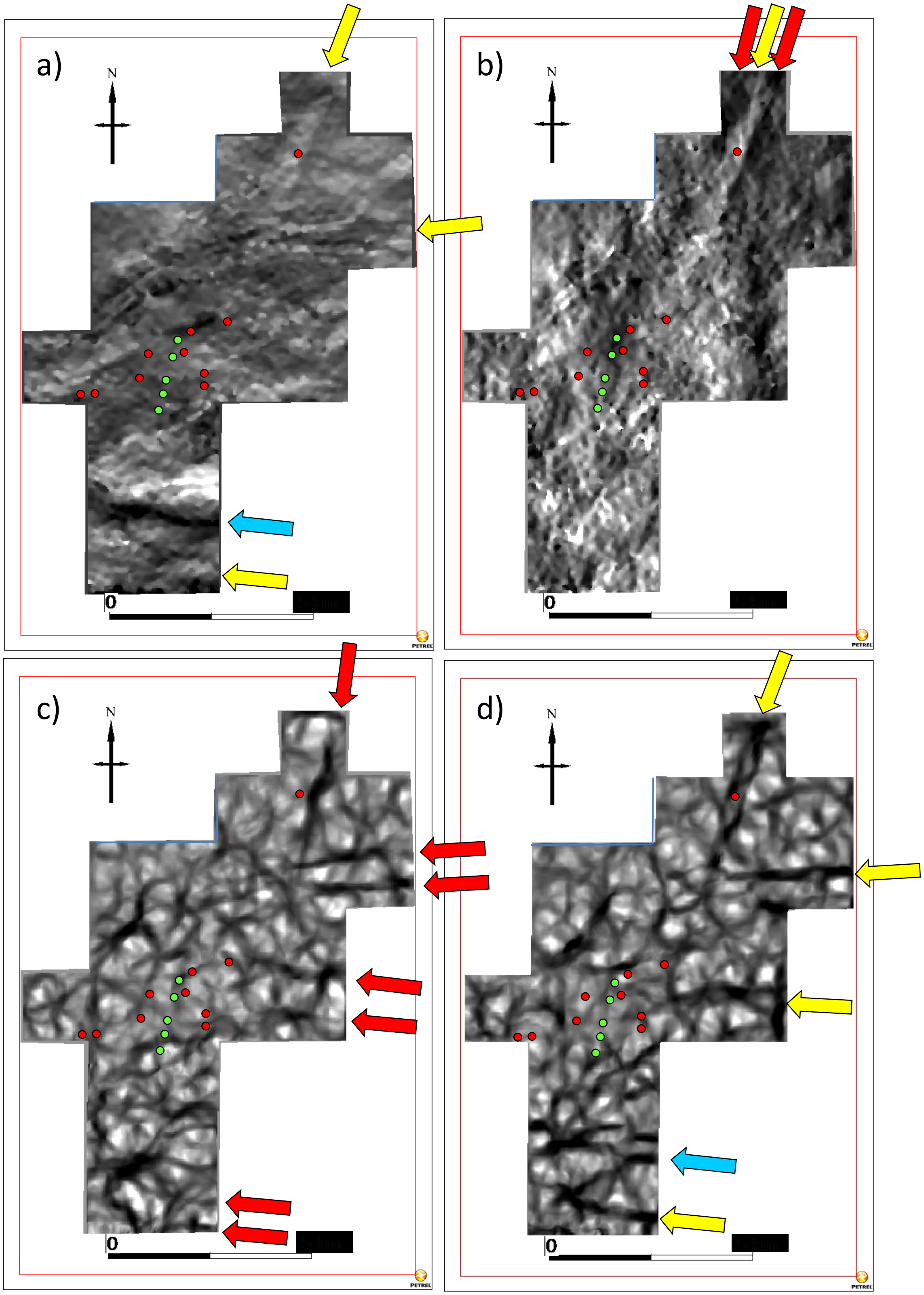

Figure 10. a) Inline (N-S) dip b) crossline (E-W) dip c) most positive principal curvature d) most negative principal curvature. Channel suggesting trends are highlighted by yellow arrows, while banks are highlighted by red arrows. The cyan arrows depict a graben. RF producing wells are indicated by green dots while non RF producing wells are indicated by red dots. The producing wells seem to follow a channel bank trend (10 c). Seismic data courtesy of CCG-Veritas.

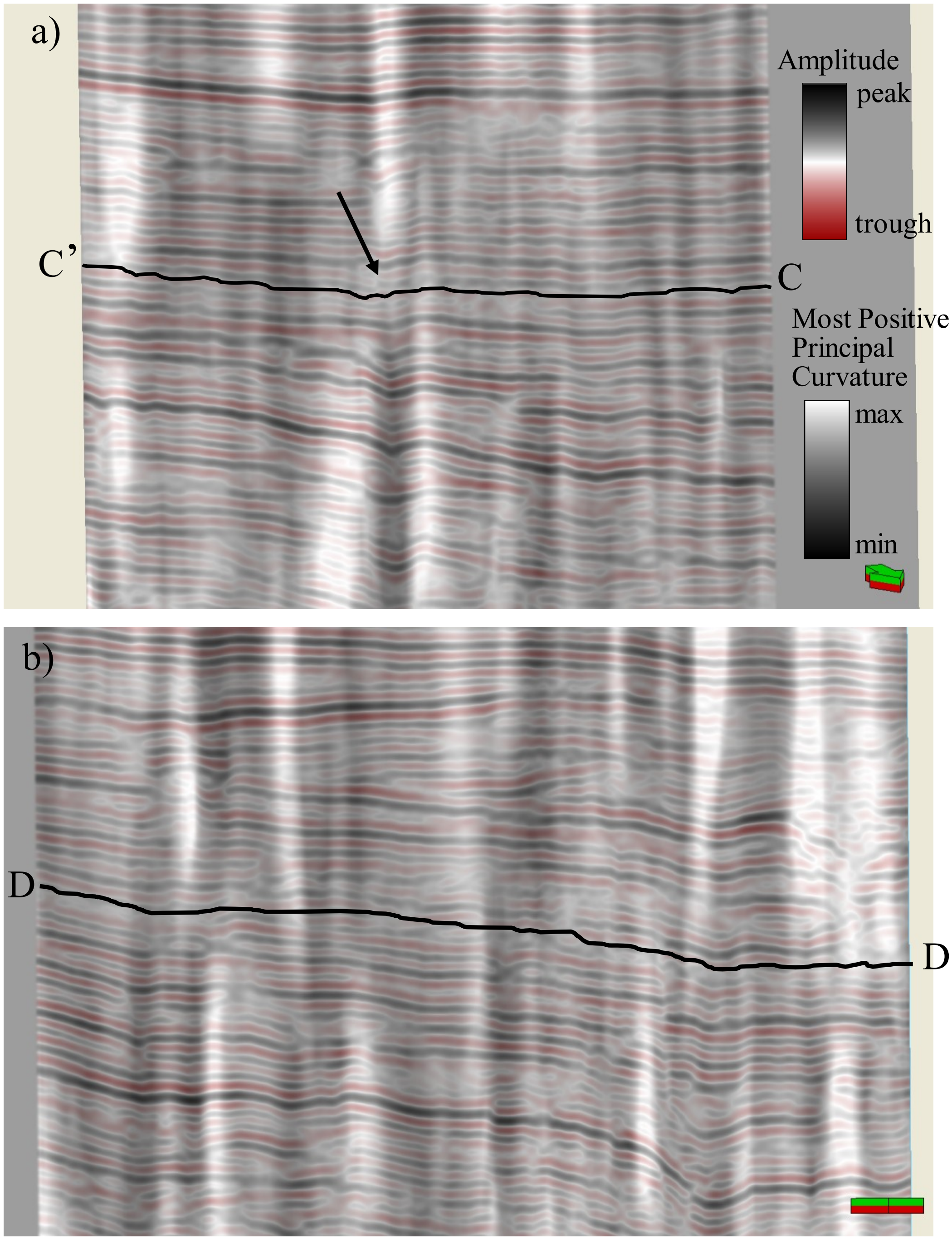

Figure 11. a) Vertical slices through most positive principal curvature co-rendered with seismic amplitude: b) line CC' and c) line DD'. The surface displayed is the Red Fork production. Positive curvature, such as the trend the RF producing wells followed in Figure 10c, are indicated in white. The channel location indicated in Figure 6 (black arrow) again shows a curvature flip above and below the horizon. Seismic data courtesy of CCG-Veritas.

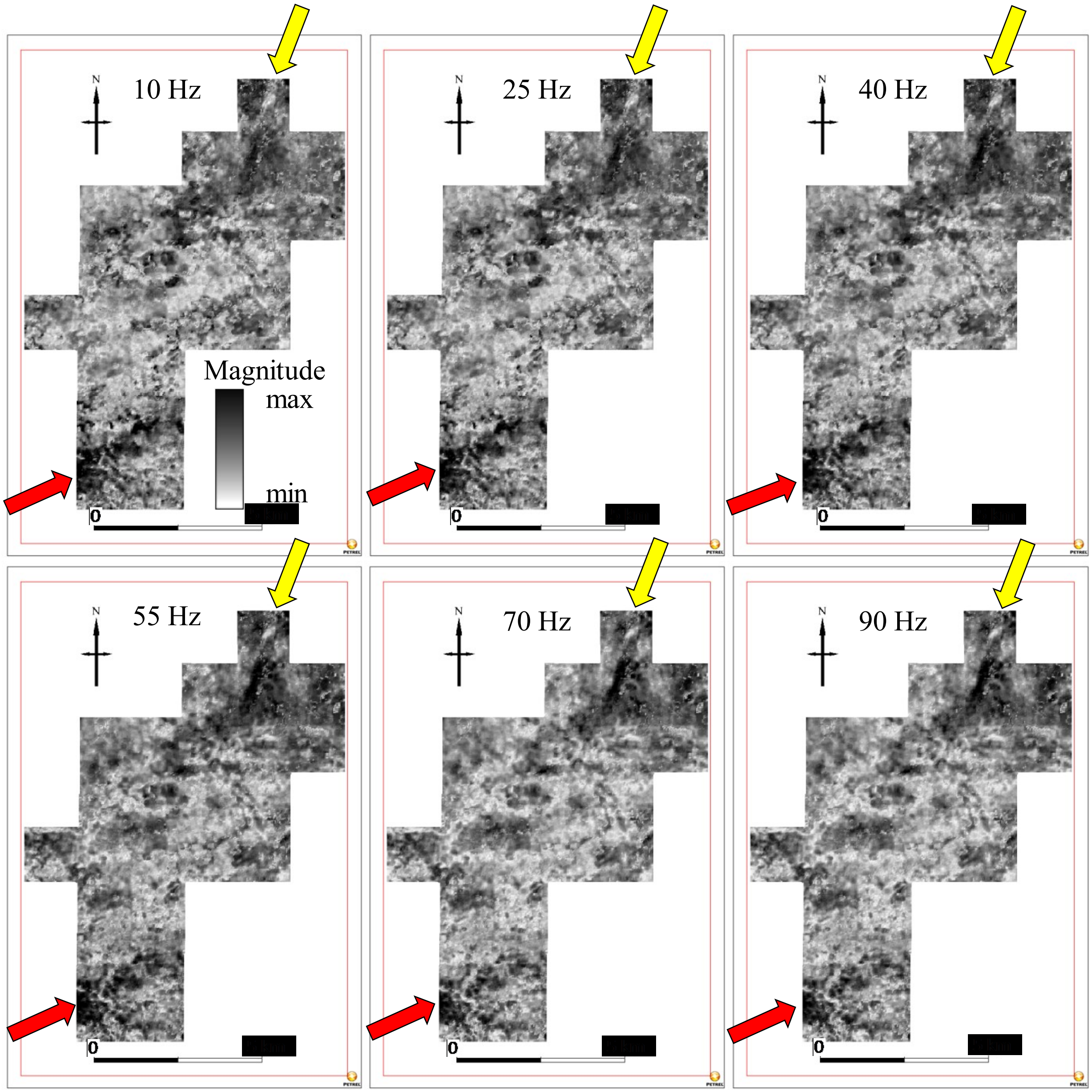

Figure 12. Horizon slices along the producing RF horizon through spectral magnitude volumes computed from the seismic amplitude. The channel indicated by the yellow arrows can be identified throughout the frequency spectrum but is stronger in the high frequencies. The wide channel like feature seen in the south (red arrows) runs through a graben and could have structural bias. It has a stronger representation in the lower frequencies. Seismic data courtesy of CCG-Veritas.

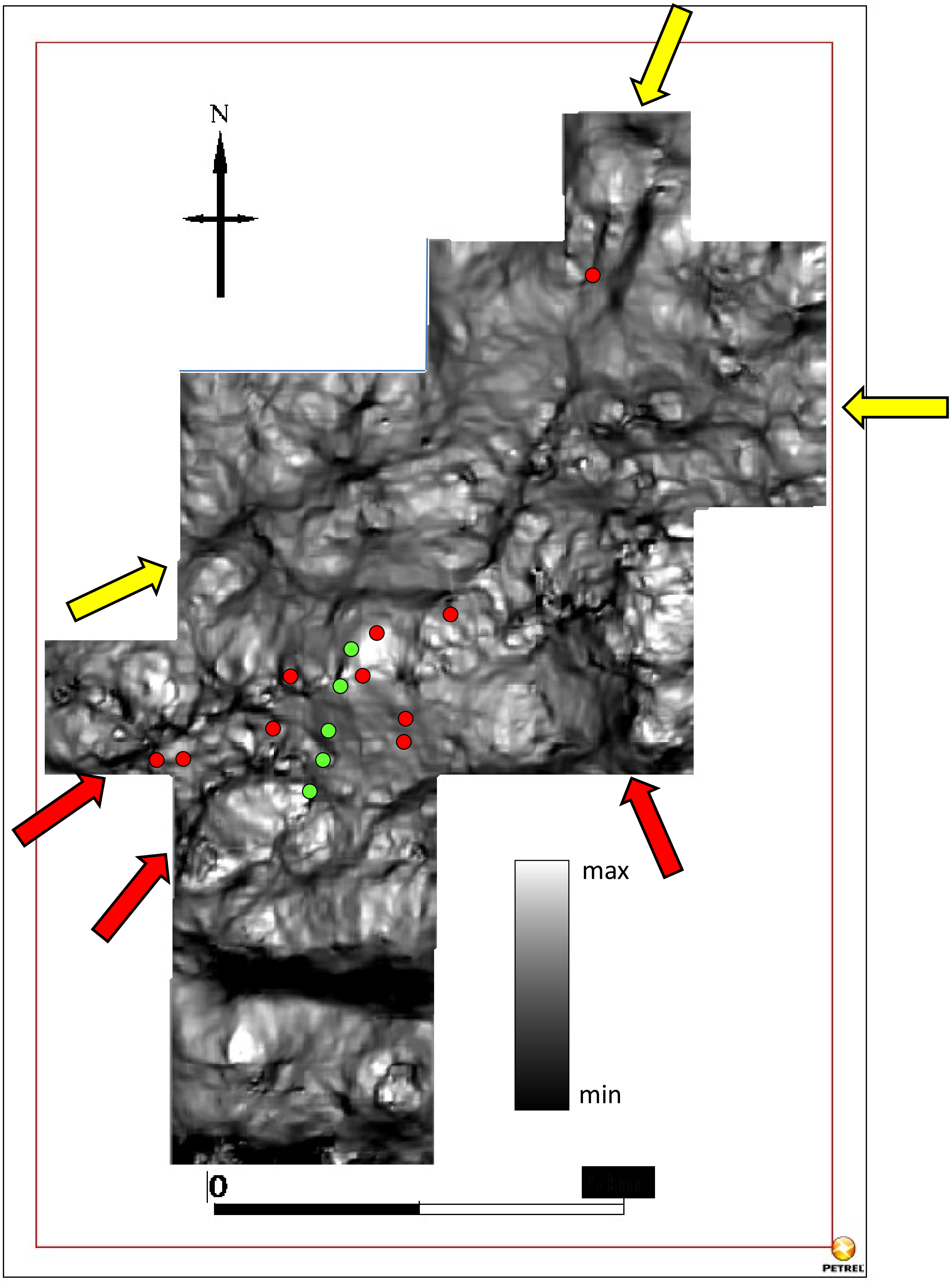

Figure 13. b) Horizon slice along the producing RF horizon through the most negative curvature of the acoustic impedance which will delineate impedance lows. While some channel suggesting trends have been previously identified in other attribute volumes (yellow arrows), new channel trends are also visible (red arrows). Seismic data courtesy of CCG-Veritas.

	V_P (m/s)	V_S (m/s)	RHOB (g/cm^3)	G (kPa)	K_e (kPa)
Pink Lime	3406.8	1810.8	2.41	7.911	17.452
Red Fork sandstone	4638.8	2899.9	2.53	21.22	26.048
Red Fork shale	3590	1888.7	2.52	8.99	20.502

Table 1. P-velocity, S-velocity , bulk density, shear modulus, and bulk modulus of key formations above and below the Red Fork channel.

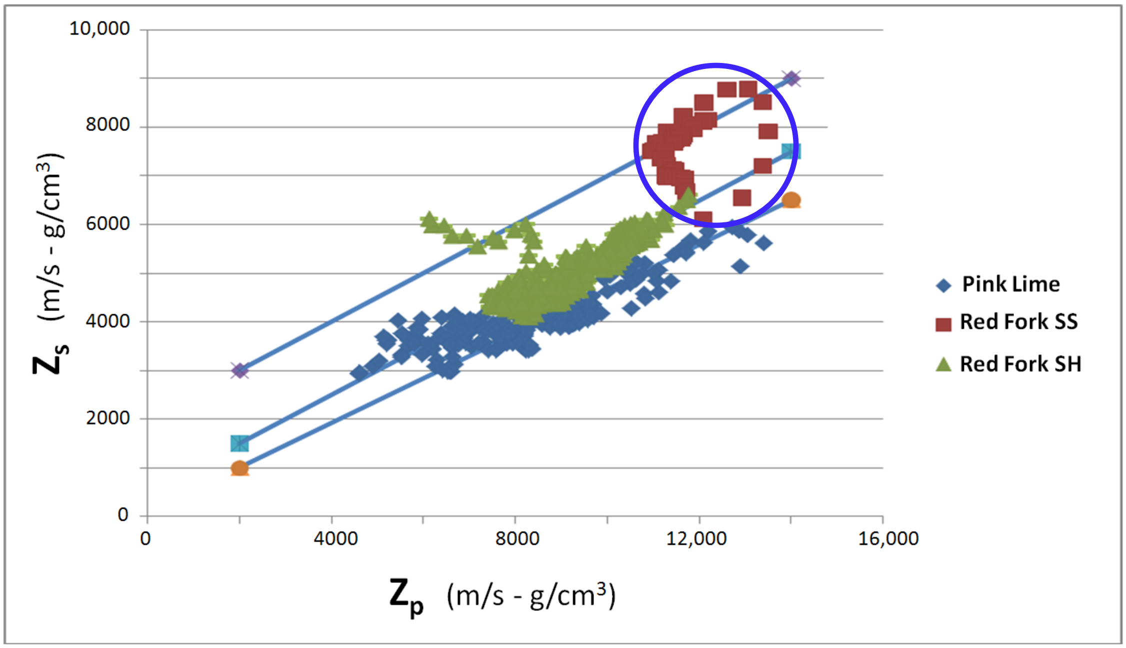

Figure 14: This figure shows the P-wave and S-wave impedance for the Red Fork shale directly below the channel and the Pink Lime directly above the channel. The channel sands can be clearly differentiated at Z_P and Z_S values that fall within the blue circle. The Red Fork shale and the Pink Lime would be difficult to differentiate cleanly without the aid of color.

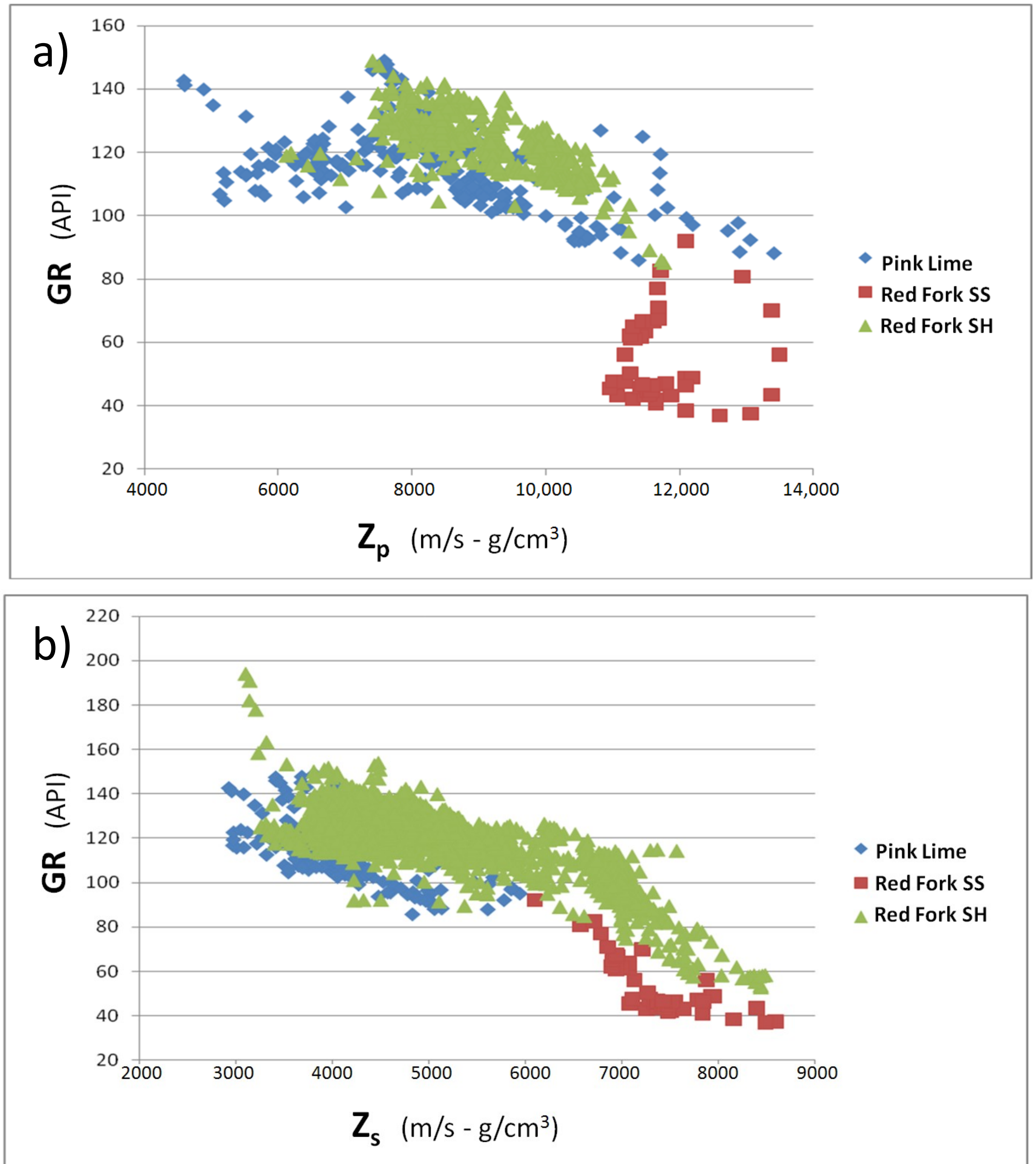

Figure 15. a) Z_p vs gamma ray for Red Fork non-producing well. The Red Fork sandstone (SS) are clearly differentiated from the Pink Lime and Red Fork shale (SH) with gamma ray values below 90 corresponding to impedance values of 11-14. b) Z_s vs gamma ray for Red Fork non-producing well. Even though there is a visible trend in the data sets, it would be hard to differentiate individual data points without using color as a guide.

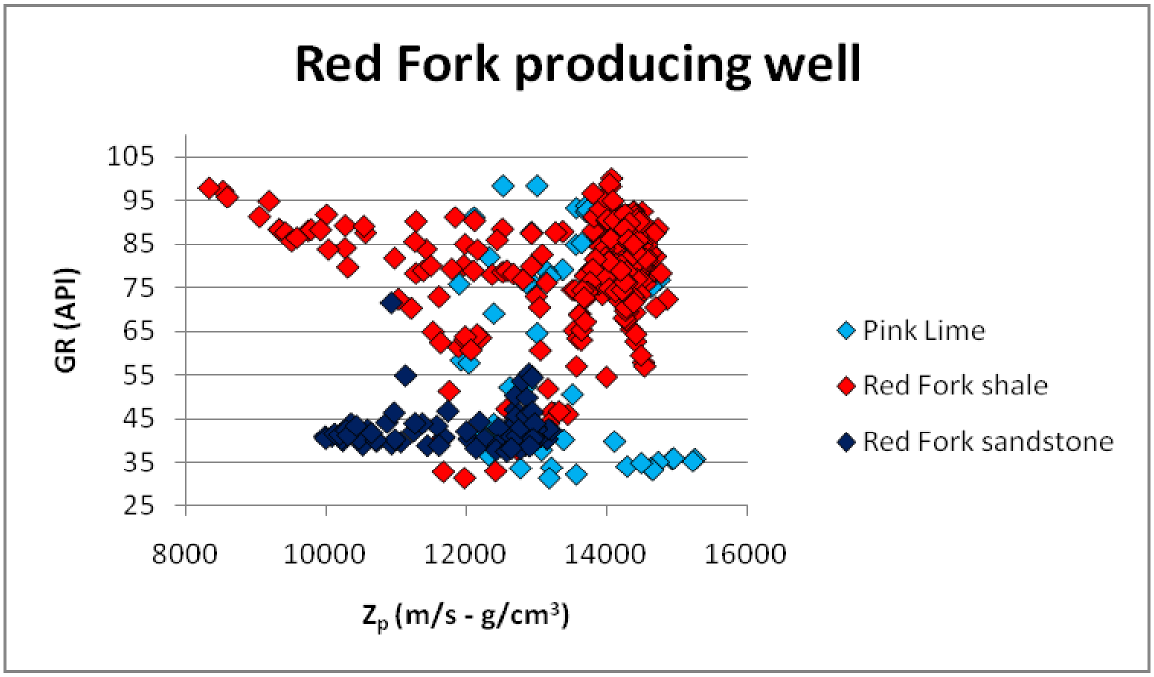

Figure 16: This figure shows the acoustic plotted against the gamma ray. The channel sands overlap both Red Fork shale and Pink Lime values, though the clustering of the sandstone from the shale could possibly be enough to differentiate the two. Overall, the sandstone can be differentiated at gamma ray values between 35 and 55 API. Unfortunately, to have gamma ray values a well has to already be in place. Acoustic impedance would not be a good filter for differentiating Red Fork sandstone, Red Fork shale, or the Pink Lime.

	Rutherford and Williams, 1989	Greenberg and Castagna, 1992
SANDSTONE	$V_S = 0.860*V_P - 3570$ (ft/s)	$V_S = 0.8042*V_P - 0.8559$ (km/s)
SHALE	$V_S = 0.7840*V_P - 2931$ (ft/s)	$V_S = 0.7697*V_P - 0.8673$ (km/s)

Table 2: The formulas used to approximate the shear velocities to use in the AVO calculations are displayed above.

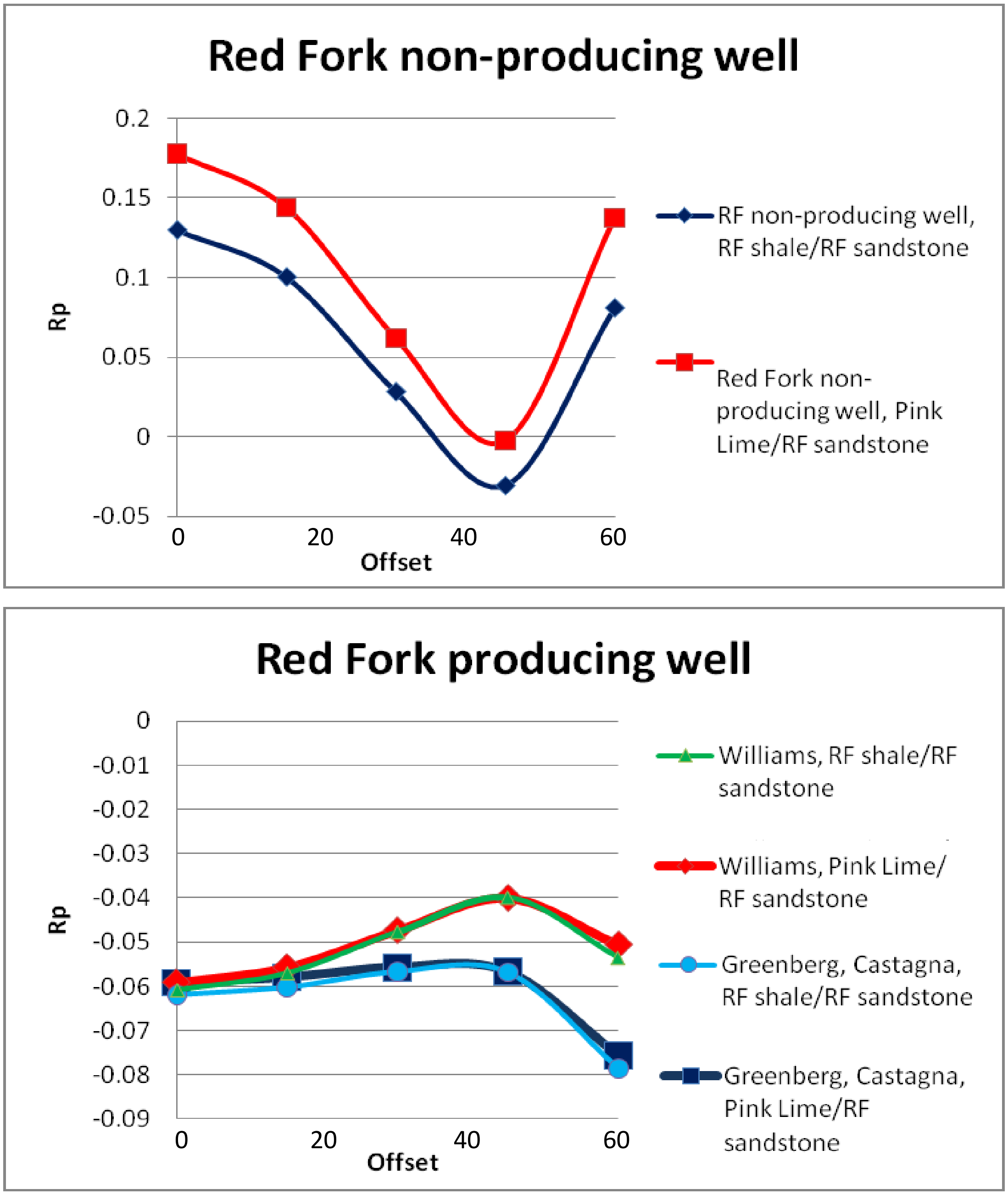

Figure 17: a) Reflectivity with offset for a Red Fork non-producing well and b) for a Red Fork producing well. The non-producing well displays class I AVO character with the strongest reflection coefficients at near offsets (≤ 15). However, the producing well displays class three AVO with the highest reflection coefficients at far offsets (30-45) using V_S values approximated from either Rutherford and Williams (1989) or Greenberg and Castagna (1992). The reflectivity difference for the producing well is minor between the near and far offsets when compared with the reflectivity difference for the non-producing well. At far offsets the non-producing wells and producing wells will have the same reflection coefficients. For differentiating the producing channel systems from the non-producing channel systems near offsets will offer the greatest variation between reflection coefficients.